Ignition conditions for magnetically insulated tamped ICF targets in cylindrical geometry

A.J. Kemp, M.M. Basko*, J. Meyer-ter-Vehn
Max-Planck-Institut für Quantenoptik,
Garching, Germany

Abstract. The ignition conditions of cylindrical ICF targets, magnetically insulated and inertially confined by a tamper, are investigated by means of one dimensional hydrodynamic simulations. The central point of interest is the effect of the tamper on the minimum fuel ρR value required for igniting pre-assembled fuel configurations. These configurations are studied for complete suppression of heat conduction losses and full re-deposition of alpha particles in the fuel due to the magnetic field. It is found that the value of ρR required for ignition depends significantly on the tamper volume and the tamper entropy at stagnation, and that it scales with the fuel mass m per unit length as $(\rho R)_{ign} \propto m^{-\kappa}$, where $0.65 \leq \kappa \leq 1.0$.

1. Introduction

Magnetized target fusion (MTF) stands for inertial confinement fusion (ICF) with an additional magnetic field; it has been discussed mostly in the context of spherically symmetric implosions [1–4]. The recent interest in cylindrical configurations [5–7] arises in the context of heavy ion fusion, where a cylindrical geometry is the natural choice in view of the cylindrical geometry of the beam.

A major drawback of target implosions in cylindrical geometry is that, under similar constraints on symmetry and stability, cylindrical implosions are less efficient in compressing the fuel than spherical ones [6]; hence they result in lower values of the fuel ρR at stagnation. This would be acceptable as long as the fuel can be ignited. Once ignition can be achieved at low values of fuel ρR, the benefit is a significant reduction of the required driver power [4, 7] compared with the usual ICF.

In order to make ignition at low ρR possible, one has to reduce the energy losses out of the fuel. A natural way to do this is to apply an external magnetic field in the target in the axial or azimuthal direction. In particular, it has been shown in Ref. [7] that ignition can be achieved at significantly reduced ρR values if the gyroradius of the 3.5 MeV alpha particles in the magnetic field is of the same order as the fuel radius at stagnation, always on the assumption that the fuel is sufficiently confined.

Sufficient external confinement of the fuel turns out to be of crucial importance in operating ICF targets at reduced ρR values. In this article we investigate the role of confinement for tamped fuel volumes at low ρR. We assume the fuel plasma to be magnetically insulated, which means that heat conduction losses as well as diffusion of alpha particles are suppressed along the radial direction. Our main conclusion is that the fuel ρR necessary for ignition depends significantly on the fuel mass, the tamper volume and the tamper entropy at stagnation.

We present the results of one dimensional computer simulations of pre-assembled fuel–tamper configurations. Similar configurations, without magnetization, have been widely studied for spherical geometry [8]. Here, we reconsider this matter for magnetized cylindrical targets to assess their potential for ICF. We will not consider questions of implosion symmetry and stability in this article.

2. Basic assumptions

Since ignition of ICF targets occurs approximately when the target implosion has come to a halt, one can, as a first step, investigate the basic properties of the ignition process by starting with pre-assembled fuel–tamper configurations at the time of stagnation. Such a configuration consists of hot deuterium–tritium (DT) fuel surrounded by a layer of dense tamper material to provide inertial confinement. We assume that the pressure is constant throughout the compressed core at the time of stagnation [9], and that the profiles of density and temperature are

* *On leave from:* Institute for Theoretical and Experimental Physics, Moscow, Russian Federation.

uniform in the fuel and the tamper layer. This simplifying assumption is consistent with one dimensional simulations of cylindrical implosions.

2.1. Target magnetization

The aim of this article is to explore the influence of a tamper on the ignition threshold of magnetized targets in the most favourable situation concerning the effect of the magnetic field. Therefore we work in the limit of high magnetic fields, such that electron and ion heat conduction, as well as diffusion of alpha particles along the radial direction, are suppressed. This limit is adequate if the collision frequencies of the alpha particles and electrons are small compared with the corresponding cyclotron frequencies. The energy relaxation time between the alpha particles and the electrons is not affected by the magnetic field [10, 11].

There is a wide range of fuel parameters where the effects of magnetic field pressure on plasma dynamics can be neglected. In this situation, we can account for magnetic field effects simply in terms of modified coefficients for heat conduction and alpha particle diffusion, and perform purely hydrodynamic, rather than full MHD simulations.

2.2. Initial configuration and basic parameters

Figure 1 shows a schematic picture of the initial configuration. It consists of a cylindrical volume of hot DT fuel, surrounded by a tamper shell of heavy metal at a high density ρ_t, and temperature T_t. The pressure p_0 is uniform throughout the fuel and the tamper. We characterize the tamper thickness by the ratio ξ_t of the outer tamper radius to the outer fuel boundary at stagnation. In order to account for different heating situations of the tamper during target implosion, we vary T_t in the range from 1 to 100 eV.

Throughout this article, we describe the fuel in terms of its stagnation temperature T_0, the fuel confinement parameter ρR and the fuel mass per unit length $m = \pi\rho R^2$. The initial fuel temperature T_0 can be chosen at any reasonable margin with about a factor of 1.5–2 above the lower limit for the ignition temperature of ICF targets, which is at approximately 4.5 keV [12]. This limit is determined by the power balance between alpha particle energy deposition in the DT fuel and losses due to bremsstrahlung radiation. The radiation can pass freely through the

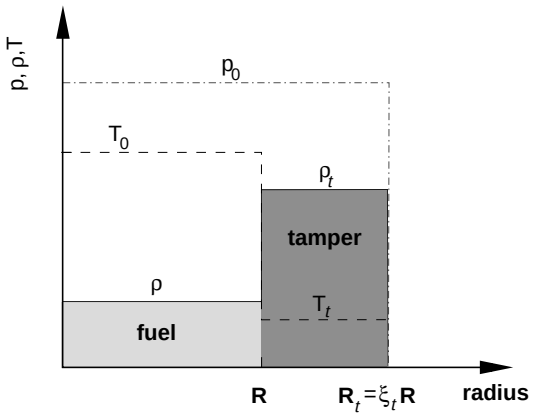

Figure 1. Radial profiles of pressure, density and temperature in the initial configuration, assuming a cylindrical geometry. The tamper thickness is characterized by the ratio ξ_t.

optically thin fuel; it heats a thin layer of the tamper next to the fuel volume and then diffuses radially outwards. We have selected our working point at $T_0 = 7$ keV, but the final results of this article are not sensitive to the exact number.

The choice of ρR and m as basic parameters, instead of $\rho = \pi(\rho R)^2/m$ and $R = m/\pi\rho R$, is made for the following reasons. For inertially confined fuel, the amount of burnt fuel (the burn fraction) depends on two times, the fusion time

$$t_f \propto 1/\rho\langle\sigma v\rangle_{DT} \tag{1}$$

where $\langle\sigma v\rangle_{DT}$ is the rate coefficient of the fusion reactions, and the confinement time $t_c \propto R/c$, where c is the sound velocity of the confining mass. The burn fraction depends on the ratio of these times,

$$t_c/t_f \propto \frac{\langle\sigma v\rangle_{DT}}{c}\rho R. \tag{2}$$

For bare fuel without any tamper, one has to take the sound velocity $c \propto \sqrt{T_0}$ of the fuel itself, which depends only on the temperature T_0, just as $\langle\sigma v\rangle_{DT}$, and is fixed by the ignition physics. Therefore, the burn fraction depends only on ρR, and an approximate formula is $f_b = \rho R/(H_B + \rho R)$, where the burn parameter H_B depends on temperature; one finds $H_B = 6.3$ g/cm^2 for $T_0 = 7$ keV [13]. Concerning tamped cylindrical configurations, the essential difference is that the relevant sound velocity is that of the tamper, and the corresponding burn fractions will be discussed later. The fuel mass m, which is the other main parameter, determines the initial amount of thermal energy in the fuel $E = \epsilon_{DT} m T_0$, with $\epsilon_{DT} = 1.15 \times 10^8$ J g^{-1} keV^{-1}.

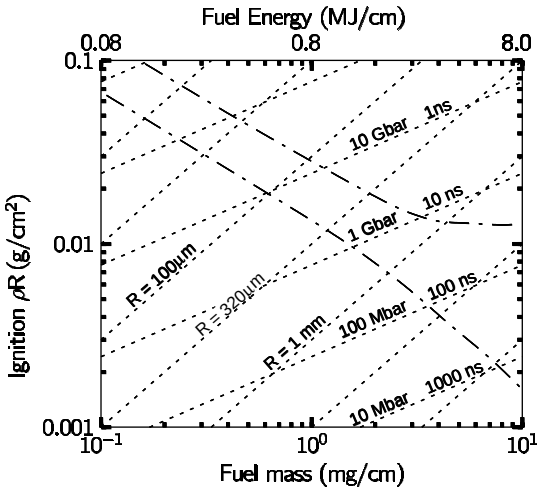

Figure 2. Initial pressure and fuel radius in terms of the principal fuel parameters. The chain curves refer to the two outer ignition curves of Fig. 6. The corresponding fuel energy ($T_0 = 7$ keV) is given on the upper axis. Additionally, the fusion timescale as defined in Eq. (1) is given. The implosion timescale is typically larger by a factor of 10–100.

In this article, the results will be plotted as functions of ρR and m. For reference, Fig. 2 shows the relevant fusion times, see Eq. (1), pressures and fuel radii in the $(\rho R, m)$ plane. The upper axis indicates the initial energy of the compressed fuel. The chain curves in Fig. 2 refer to the outer ignition curves of Fig. 6. They will be discussed in Section 3.3.

3. Results

The simulations described below were performed with the Lagrangian, one dimensional hydrodynamics code DEIRA [14], featuring three temperatures for electrons, ions and radiation, real matter equation of state (EOS) and opacity tables, and thermonuclear reactions. Non-local deposition of the fast alpha particles in the fuel is modeled by a diffusion equation [10, 11].

In order to account for the magnetic insulation of the target in the sense discussed in Section 2.1, the diffusion coefficient for fast alpha particles and the coefficients for both ionic and electronic heat conduction are set equal to zero in the code, while the finite 'heat capacity' of the alpha particles is retained.

3.1. Optimum tamper thickness

The dependence of burn fraction and energy gain on tamper thickness ξ_t are shown in Fig. 3 for

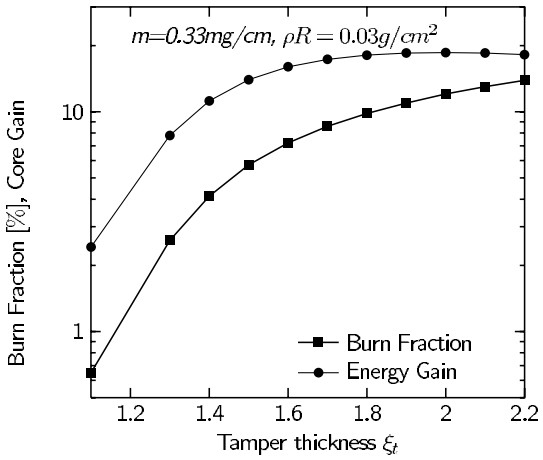

Figure 3. Fuel burn fraction and energy gain of magnetically insulated targets versus tamper thickness ξ_t. In this and Figs 4–6, each symbol represents the final result of a hydrodynamic simulation run.

typical values of ρR and m. The energy gain is defined here as the ratio of the thermonuclear energy yield to the energy of the configuration at stagnation, including the tamper energy. For thin tampers, the energy gain increases rapidly with ξ_t; for large values of ξ_t, the energy gain and burn fraction both saturate and the energy gain even falls slightly. The saturation of the energy gain for large tampers results from the high fraction of energy invested in the tamper. This energy fraction, given approximately by $\xi_t^2 - 1$, is the ratio of the tamper to the fuel volume at stagnation. Since the configuration is assumed to be isobaric initially, the ratios of energies and volumes of fuel and tamper are approximately equal.

As a working point near the optimum, we have chosen $\xi_t = 1.7$, corresponding to a tamper volume twice the fuel volume and a temperature of $T_t = 100$ eV. It will be shown later how the final results are affected by the choice of tamper thickness and temperature. In all the simulation results presented here, we have used gold as the tamper material, but any other heavy metal will give similar results.

3.2. Fuel burn in magnetically insulated targets

In Fig. 4, the burn fraction of the fuel–tamper configurations with and without magnetic insulation is plotted as a function of fuel ρR value. One observes a dramatic increase of the fuel burn fraction at low ρR for the magnetized case. Another distinct feature is the lack of a sharp ignition boundary. The burn frac-

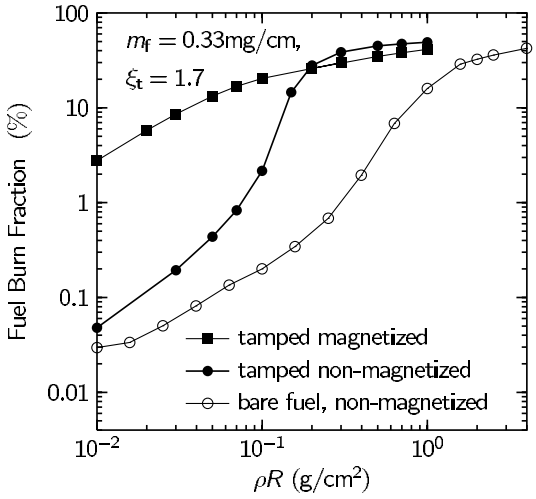

Figure 4. Fuel burn fraction versus initial fuel ρR of targets with and without magnetic insulation. The open circles represent the results for the case of bare fuel without magnetic insulation.

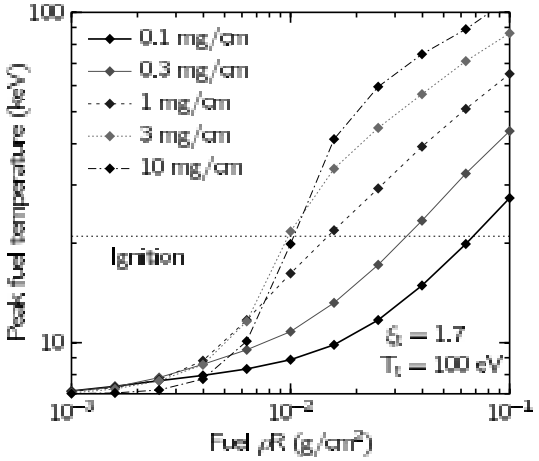

Figure 5. Peak fuel temperature during target disintegration versus the initial fuel ρR, for targets with various fuel masses m. The ignition threshold, as defined in Section 3.3, is indicated by the horizontal line.

tion increases gradually with fuel ρR value, similar to the burn in magnetically confined fusion plasmas. The reason for this is the complete re-deposition of alpha particles in the fuel, even at low fuel ρR values.

In non-magnetized targets, however, there is an 'ignition cliff', a marked increase of the burn fraction when passing a certain ρR threshold as seen in Fig. 4. This results from the bootstrap heating by alpha particles when the fuel ρR value exceeds a stopping range of approximately 0.3 g/cm^2. For smaller ρR values and without a magnetic field, most of the alpha particles leave the fuel.

Additionally, Fig. 4 shows the fuel burn fraction of bare fuel without tamper and magnetic insulation, corresponding to the situation discussed in Section 2.2. Without the additional confinement owing to tamper, the ignition cliff moves to larger fuel ρR values and becomes less sharp.

3.3. Ignition of magnetically insulated targets

Figure 5 shows the peak fuel temperature reached in various target explosions as a function of the initial fuel ρR value. Each point in the plot represents an individual history of a target evolution with given initial values of fuel mass m and ρR; the curves connect points of constant fuel mass. Targets are called ignited if the peak fuel temperature during disintegration exceeds 21 keV, i.e. if the fuel temperature rises to at least three times the initial value of $T_0 = 7$ keV. Here we need such a definition since there is no clear ignition cliff, as in the case of non-magnetized targets (Figs 4 and 5). This is consistent with the ignition threshold of non-magnetized targets. In Fig. 5 one observes that the ignition threshold moves systematically to lower fuel ρR values as the fuel mass increases.

The dependence of the ρR ignition threshold on fuel mass is shown explicitly in Fig. 6. Various curves are presented for different values of the tamper parameters in order to account for different implosion histories. The scalings of the ignition threshold ρR with the fuel mass $(\rho R)_{ign} \propto m^{-\kappa}$, where $\kappa \approx 0.65$ for small fuel mass ($\leq$1 mg/cm) and approaches $\kappa \approx 1.0$ for larger m, are indicated. It turns out that the position of the ignition threshold ρR for large fuel masses $m \geq 1.0$ mg/cm depends on the initial temperature T_t of the tamper material. For warm tampers with $T_t \approx 100$ eV, it remains above 0.01 g/cm^2. For cold tampers with $T_t \ll 100$ eV, however, it can drop significantly below this value. In this regime the fusion timescale, as given by Eq. (1) and shown in Fig. 2, is in the microsecond range.

Also shown in Fig. 6 is the dependence on tamper thickness ξ_t. The ignition ρR values of targets with a thin tamper ($\xi_t = 1.4$) and those with a large tamper ($\xi_t = 1.7$) differ by about a factor of two.

3.4. Ignition scaling with fuel mass

In this section, we want to show that the simulation results can be understood in terms of the EOS

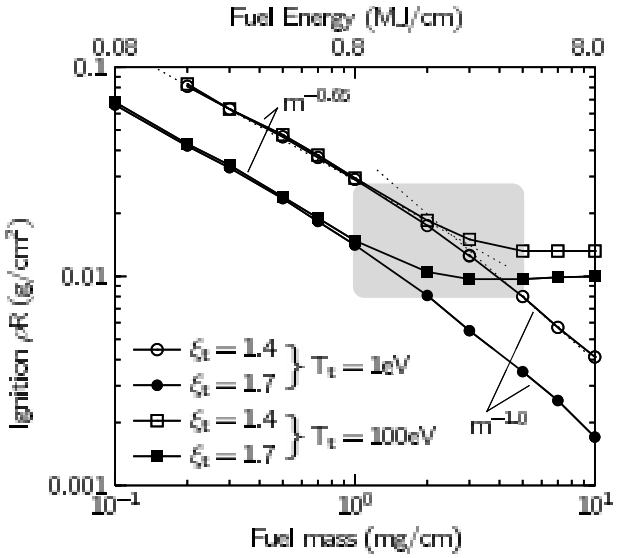

Figure 6. Ignition ρR versus fuel mass for different choices of thickness ξ_t and initial temperature T_t of the tamper. The ignition scalings at low and high fuel masses are indicated by dotted curves (Section 3.4). For the shaded area, see Section 4.

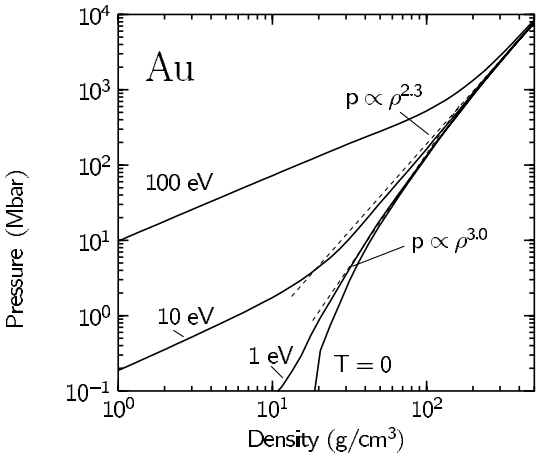

Figure 7. Gold pressure isotherms for $T = 0$, 1, 10, 100 eV, taken from the EOS table which has been used for the numerical simulations. The scalings responsible for the ignition scalings of Fig. 6 are indicated by dashed lines.

properties of the tamper. For the tamped configuration, the confinement time t_c is essentially the time of tamper disintegration. Therefore, the ignition scaling is found from Eq. (2) for a fixed ratio t_c/t_f in the form

$$(\rho R)_{ign} \propto c_t \tag{3}$$

where $c_t \propto (dp/d\rho)_t^{1/2}$ is now the sound velocity of the tamper, determined by its EOS. The pressure EOS for gold, which is the tamper material used in the simulations, is shown in Fig. 7 in the form of four isotherms. One can distinguish two regions. Firstly, the 'degenerate' regime close to the $T = 0$ isotherm, where the pressure can be approximated by $p \propto \rho_t^\gamma$ with $2.3 \le \gamma \le 3.0$ in the relevant density and temperature regime, and, secondly, the thermal regime where $p \propto \rho_t T_t$.

In order to express c_t in terms of the fuel ρR value and mass m, we make use of our assumption that initially the pressures in the fuel and tamper layers are equal and find

$$\rho T_0 \propto p \equiv p_t \propto \begin{cases} \rho_t^\gamma & \text{(degenerate regime)} \\ \rho_t T_t & \text{(thermal regime)} \end{cases} \tag{4}$$

for the initial configuration, where p_t, ρ_t and T_t refer to the tamper, and p, ρ and T_0 to the fuel. For the degenerate regime, one obtains $c_t \propto \rho_t^{(\gamma-1)/2} \propto \rho^{(\gamma-1)/2\gamma}$, and from Eq. (3) together with $m \propto \rho R^2$

$$(\rho R)_{ign} \propto m^{-\kappa} \tag{5}$$

with $\kappa = (\gamma - 1)/2 = 0.65$ for $\gamma = 2.3$ and $\kappa = 1.0$ for $\gamma = 3.0$. Apparently, these values of κ explain the shapes of the ignition curves in Fig. 6 for cold tampers ($T_t = 1$ eV). For higher temperatures ($T_t =$ 100 eV), the tamper is in the thermal regime with $c_t \propto \sqrt{T_t}$, and Eq. (3) therefore leads to

$$(\rho R)_{ign} = \text{const} \tag{6}$$

independent of fuel mass. This explains the lower bound of $(\rho R)_{ign} \approx 0.01$ g/cm^2 seen in Fig. 6 for $m \le 1$ mg/cm and $T_t = 100$ eV.

For a more quantitative understanding of the dependence of the constant in Eq. (6) on ξ_t and T_t, one would have to analyse the tamper dynamics in more detail. Here, we emphasize only the central result that the $(\rho R)_{ign}$ values of tamped fuel configurations have in principle no lower bound in the parameter region of interest for ICF ($m \le$ 10 mg/cm), at least not in a one dimensional treatment, provided that the tamper material can be kept at low entropy during the implosion.

Let us finally remark that the result (5) could be written alternatively in the form $\rho^{(\gamma+1)/2\gamma} R = \text{const}$, which is the invariant for the degenerate regime. In this presentation, ignition of magnetized cylindrical targets with cold tampers scales with $\rho^{2/3} R$, setting $\gamma = 3$.

4. Summary and conclusions

As already discussed in previous publications [1–4, 7], the presence of a strong magnetic field in ICF targets can significantly reduce the requirements on the fuel ρR at ignition, compared with non-magnetized targets (where $\rho R \geq 0.3$ g/cm^2 for hot spot ignition). The role of the magnetic field in the MTF ignition mode is to reduce heat conduction losses and to retain the 3.5 MeV alpha particles. However, even in the optimal case of targets with no heat conduction losses and complete alpha particle re-deposition, inertial confinement of the fuel results in a lower limit on the ignition ρR value.

In this article, we have investigated ignition conditions of magnetically insulated cylindrical fusion targets by exploring the dynamics of fuel–tamper configurations after stagnation. This has been done by means of one dimensional hydrodynamic simulations, where we have completely suppressed the effects of heat conduction and the diffusion of alpha particles. The results show that the minimum ρR value necessary for ignition depends significantly on fuel mass, tamper volume and tamper entropy:

(a) For a fixed tamper entropy and fractional volume, ignition occurs only when a minimum fuel ρR value is reached at stagnation. The value of the fuel ρR at ignition scales with the fuel mass m per unit length as $m^{-\kappa}$, where $0.65 \leq \kappa \leq 1.0$ depending on fuel mass.
(b) The $(\rho R)_{min}$ saturation level decreases with decreasing tamper entropy, but this leads us to higher fuel masses beyond the scope of ICF.
(c) Larger tampers can also help to reduce the value of ρR required for ignition.

Our results can give good guidance over a vast parameter space when designing cylindrical MTF targets. A possible window for MTF operation with heavy ion beams is indicated by the shaded area in Fig. 6. The boundaries have been selected such that the lowest possible value of $(\rho R)_{ign}$ is obtained at fuel energies of a few MJ/cm, which may be available from future heavy ion drivers. The window corresponds to fuel radii up to 1 mm and pressures below 10 Gbar, as one may see from Fig. 2. A simple estimate of the target implosion time necessary to reach such parameters gives times of the order of 100 ns at a convergence ratio of $C_r = 10$. This is consistent with the pulse times of heavy ion beam drivers. Compared with non-magnetized ICF targets, magnetization of cylindrical DT targets allows the ignition ρR threshold to be reduced by at least a factor of 10–30, depending on the implosion history. Since the driver power necessary for breakeven in cylindrical ICF targets scales as $P_{dr} \propto (\rho R)^2_{ign}$ [7], this leads to a significant reduction in the required driver power for heavy ion beam driven, magnetized cylindrical targets in the MTF ignition mode.

As the ignition scheme discussed in this article operates essentially in the volume ignition mode, one cannot expect high gains without additional modifications to the target structure, such as the non-homogeneous targets proposed by Churazov et al. [5]. These targets consist of a 'hot' section at one end of the target and a 'cold' section at the other end. The hot section is characterized by a low fuel ρR value and a high temperature. It is used to launch a burn wave that propagates along the cylinder axis towards the cold end of the target. The ignition conditions discussed will hold for the hot ignition section of the target, while the overall target gain will be enhanced by adding sections of cold fuel. It should be noted that adequate modelling of such targets requires rather sophisticated two and three dimensional MHD codes with anisotropic heat and alpha particle transport.

We have not considered how the assembled fuel–tamper configurations can be reached by target implosions. Neither have we considered losses through the ends of the cylindrical configuration [7] or questions of symmetry and stability. These questions, together with a more realistic implementation of the magnetic field, will have to be addressed in future investigations, which could further narrow the parameter space available for MTF.

References

[1] Lindemuth, I.R., Kirkpatrick, R.C., Nucl. Fusion **23** (1983) 263.
[2] Jones, R.D., Mead, W.C., Nucl. Fusion **26** (1986) 127.
[3] Hasegawa, A., et al., Nucl. Fusion **28** (1988) 369.
[4] Kirkpatrick, R.C., Lindemuth, I.R., Ward, M., Nucl. Fusion **27** (1995) 201.
[5] Churazov, M., Sharkov, B., Zabrodina, E., Fusion Eng. Des. **32** (1996) 577.
[6] Basko, M., Inertial Confinement Fusion with Magnetized Fuel in Cylindrical Targets, Rep. EUR-CEA-FC-1645, CEA Cadarache (1998).
[7] Basko, M.M., Kemp, A., Meyer-ter-Vehn, J., Nucl. Fusion **40** (2000) 59.
[8] Atzeni, S., Jpn. J. Appl. Phys. **34** (1995) 1980.
[9] Meyer-ter-Vehn, J., Nucl. Fusion **22** (1982) 561.

[10] Basko, M.M., Fiz. Plasmy **13** (1987) 967 [English translation: Sov. J. Plasma Phys. **13** (1987) 558].
[11] Liberman, M., Velikovich, A., J. Plasma Phys. **31** (1984) 369.
[12] Lindl, J., Inertial Confinement Fusion: The Quest for Ignition and Energy Gain Using Indirect Drive, Springer Verlag, Berlin (1998).
[13] Oparin, A.M., Anisimov, S.I., Meyer-ter-Vehn, J., Nucl. Fusion **36** (1996) 443.
[14] Basko, M.M., Nucl. Fusion **30** (1990) 2443.

(Manuscript received 26 June 2000
Final manuscript accepted 14 December 2000)

E-mail address of A.J. Kemp: kemp@mpq.mpg.de

Subject classification: L0, It